Cavitation Effect towards Graphene Oxide Synthesis using Liquid Phase Exfoliation Method Assisted by Linear Alkylbenzene Sulfonate

Duwi Susanto, Salsabila Husna, and Wipsar Sunu Brams Dwandaru*
Physics Education Department, Faculty of Mathematics and Natural Sciences, Universitas Negeri Yogyakarta, Colombo Street No. 1, Yogyakarta, 55281

Abstract: In this study, graphene oxide was synthesized using the liquid phase exfoliation method. Graphene oxide synthesis was carried out by dispersing graphite powder in deionized water and adding linear alkylbenzene sulfonate surfactant, followed by exposure to ultrasonic waves at a frequency of 21 kHz. The graphite exfoliation process in this method took advantage of the cavitation phenomenon that occurred during the sonication process. The cavitation effect in this research was observed based on the characterization results of graphene oxide. The ultraviolet-visible spectroscopy results indicated that cavitation events influenced the emergence of the main absorption peak at a wavelength of 240 nm and a secondary peak at 287 nm. The X-ray diffraction results showed a phase transition from crystalline graphite to an amorphous phase, as indicated by the disappearance of sharp graphite peaks and the appearance of broad peaks at $2\theta \cong 18^{\circ}$. The Fourier transform infrared analysis showed that cavitation added oxygen groups to the graphene oxide produced, e.g.: -OH and C-OH, whose intensities increased after sonication. Scanning electron microscope analysis revealed sheet-like structures on the graphite surface. Based on the energy dispersive X-ray results, the C/O ratio of the graphene oxide sample was 68.99%. This aforementioned result supported the Fourier transform infrared results where an increase in the oxygen composition occurred after the sonication.

Keywords: Graphene oxide; Linear alkylbenzene sulfonate; liquid phase exfoliation; ultrasonication.

*Corresponding author: wipsarian@uny.ac.id

http://dx.doi.org/10.12962/j24604682.v21i1.20096
2460-4682

I. INTRODUCTION

One essential and interesting material to be studied is carbon-based nanomaterials. Carbon is a large class of materials that have several allotropes with different microstructures and morphologies, e.g.: carbon nanotubes (CNT), graphene, graphene oxide (GO), mesoporous carbon, carbon nanospheres, and amorphous carbon, that can be applied in the development of environmental and energy technologies [1]. Graphene oxide (GO) is an allotrope of carbon nanostructures that can be easily obtained through the exfoliation of graphite flakes [2]. GO has been widely applied in various fields due to its unique physicochemical properties, including large surface area, electrical conductivity, and optimal absorption capacity [1,3]. On the surface and edges of GO, there are many oxygen functional groups, such as hydroxyl (-OH), carbonyl (-C=O-), and carboxyl (-COOH) [1-4]. Furthermore, the two-dimensional allotrope structure of graphene, which forms the basis of GO, provides excellent crystalline properties making it an attractive choice for many researchers to explore its use in various applications [3].

Based on several studies, GO exhibits high conductivity and stability due to the presence of hydroxyl or oxide groups on its surface [5, 6]. GO has a bandgap value in the ultraviolet (UV) range. Because of its suitable bandgap for UV light, GO is often used as a photodegradation material for textile dye waste [5, 6]. Despite its various superior properties, the synthesis process of GO still involves the use of hazardous and toxic chemicals. The most common and frequently used method for producing GO is the Hummer's method. However, this method still utilizes hazardous substances such as HCl, H_2SO_4, $KMnO_4$, and $NaNO_3$ [7, 8].

Liquid phase exfoliation (LPE) is a process for producing GO using a physical method, which involves grinding graphite dissolved in water. This method has the advantage of producing GO on a large scale in a relatively short time. Additionally, the production process is cost-effective and environmentally friendly as it does not involve the use of hazardous and toxic materials [9]. However, research using this method is still limited, so the use of the LPE method for large-scale production of GO has not been largely implemented. One prominent advantage of this method is its scalability and cost-effectiveness, making it very promising for large-scale GO production. Furthermore, the synthesis process using this method does not involve hazardous chemicals, making it more environmentally friendly compared to the Hummers method. However, the drawback of this method is its relatively low exfoliation efficiency compared to the Hummers method, making it a challenge to develop this method for producing high-quality GO [10-12]. Additionally, controlling the size and distribution of GO remains a challenge for future research. This study aims to further investigate this method and develop the GO exfoli-

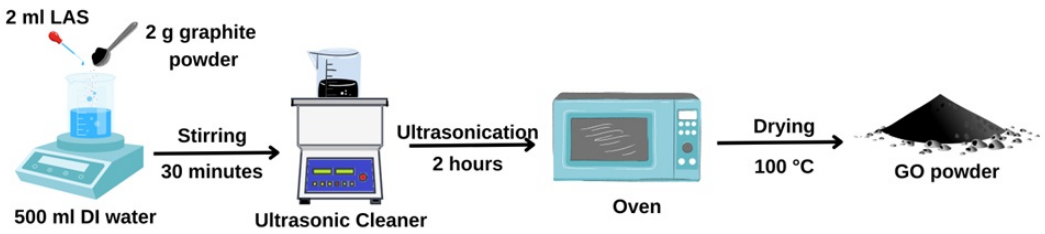

FIG. 1: GO synthesis process with ultrasonication.

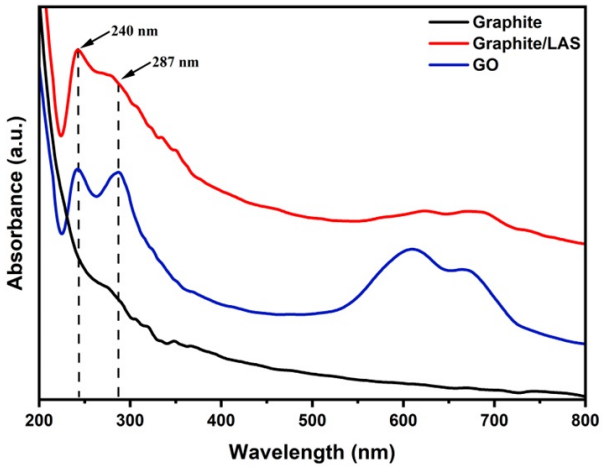

FIG. 2: UV-Vis test results of graphite, graphite/LAS (0 kHz), and GO (21 kHz) samples.

ation process.

The graphite exfoliation process in the LPE method utilizes cavitation events caused by pressure changes in the solution induced by ultrasonic waves. Cavitation is the formation of microbubbles in water due to pressure differences in the liquid. The cavitation bubbles formed then collapse rapidly, generating strong shock waves to break down the graphite [13]. The destruction of the graphite structure can facilitate exfoliation of the graphite layers. However, cavitation occurring from ultrasonic waves is generally accepted without further scrutiny [14]. Furthermore, there is still limited explanation regarding the impact of cavitation on the formation of GO. By studying the cavitation effects on the synthesized GO, it is hoped that control over the dimensions and size of GO according to desired specifications can be achieved.

In this study, linear alkylbenzene sulfonate (LAS) surfactant was added to facilitate the exfoliation process. Surfactants with hydrophilic and hydrophobic groups facilitate the dispersion of graphite powder in water. Additionally, the hydrophobic properties of the surfactant enable it to penetrate the interlayer spaces of graphene within the graphite structure. The surfactant molecules entering the interlayer spaces of graphene are expected to weaken the van der Waals bonds between the layers making it easier for them to exfoliate [15]. Previous research by Pratama et al. demonstrated that the use of LAS surfactant for graphite exfoliation can produce GO with good quality, as seen from the Raman test results [16].

II. METHOD

The materials used in the study included pure graphite powder (Sigma Aldrich), deionized water (Kimia Farma), and LAS surfactant (Kimia Farma). The equipment used in the synthesis process included: a magnetic stirrer, magnetic bar, 10 ml measuring glass, 1000 ml beaker glass, Panasonic microwave, spatula, plastic wrap, ultrasonic cleaner model UC-8360, sample bottles, 50 ml beaker glass, Osuka brand digital balance, and petri dish. The tools used for sample analysis were Shimadzu UV-2450 ultraviolet-visible (UV-Vis) spectrophotometer, Bruker D2-Phaser (X-ray diffraction) XRD instrument, Phenom Pro-x scanning electron microscope energy dispersive X-ray (SEM-EDX) instrument, and Spectrum Two System L160000A Fourier transform infrared (FTIR) spectrometer.

The synthesis process of the GO is illustrated in Fig. 1. Firstly, 2 ml of LAS solution and 2 g of graphite powder were dispersed in 500 ml of deionized water. The solution was then stirred for 30 minutes at room temperature. Subsequently, ultrasonic exposure was carried out using an ultrasonic cleaner for 120 minutes. Drying was performed using a microwave at 100°C until GO powder was obtained.

III. RESULTS AND DISCUSSION

The results of the absorbance analysis of graphite, graphite/LAS (0 kHz), and GO (21 kHz) samples are shown in Fig. 2. Based on previous research, GO material exhibits characteristic absorption peaks at a wavelength of 230 nm (main peak) and a shouldering peak at a wavelength of 298 nm [17]. In this study, the UV-Vis absorption spectrum of the graphite/LAS and GO samples shows a sharp absorption peak at a wavelength of 240 nm attributed to the $\pi \rightarrow \pi^*$ transition of the C=C aromatic bond. This peak slightly shifts from the expected peak of GO, which should be around 230 nm. After ultrasonication, a shouldering peak appears at a wavelength of 287 nm, indicating the occurrence of the n $\rightarrow \pi^*$ transition of the C=O bond. The main peak shifts slightly compared to some literatures, e.g.: [17]. This may be due to the prolonged drying process, which reduces the oxygen groups in the material causing a shift of the main absorption peak to longer wavelengths.

The bandgap energy was analyzed based on the absorbance spectrum of the samples using the Tauc plot method. The

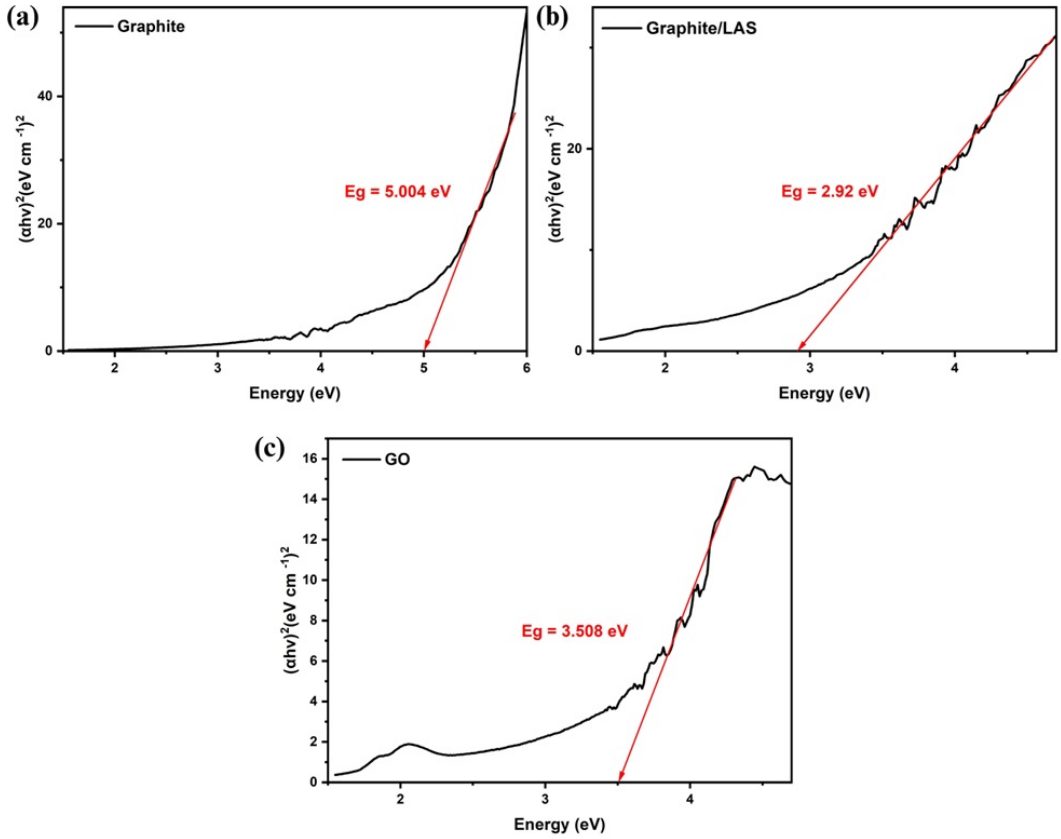

FIG. 3: Bandgap energies of graphite sample (a), graphite/LAS (0 kHz) (b), and GO (21 kHz) (c) analyzed using the Tauc plot method.

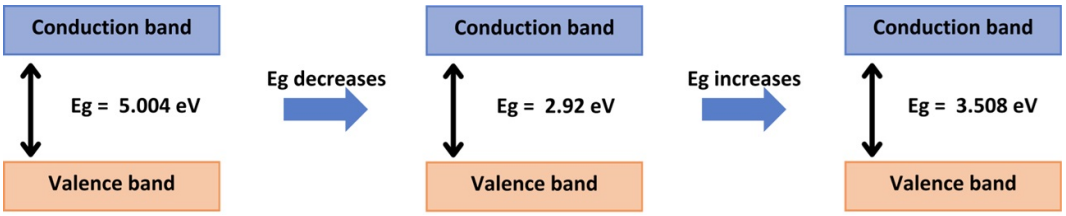

FIG. 4: Changes in bandgap energies of graphite (left), graphite/LAS (center), and GO (right).

bandgap energy of the samples can be observed in Fig. 3. Optical analysis indicates a change in the bandgap energy in the graphite sample (see Fig. 4). The graphite sample has bandgap energy of 5.004 eV, which then decreases to 2.92 eV after the addition of surfactant (0 kHz). This is due to the surfactant adhering to the surface and interlayer gaps of the graphene layers, which then act as bridges between layers and facilitate electronic transitions. After the sonication process with a frequency of 21 kHz, the bandgap energy increases to 3.508 eV due to the increase in oxygen groups in the material, which leads to a decrease in material conductivity. The change in the materials bandgap energy affects the quality of GO, such as conductivity, light absorption rate, and/or fluorescence emission. This can influence its application in specific needs.

Fig. 5 displays the XRD diffraction patterns of the graphite, graphite/LAS (0 kHz), and GO (21 kHz) samples. To enhance the diffraction peaks, the Savitzky-Golay smoothing method in the Origin software has been applied. In the XRD spectrum of graphite, several distinct diffraction peaks are observed around 26.3°, 42.3°, 44.2°, 54.4°, 59.4°, and 77.3°. These peaks correspond to the (002), (100), (101), (102), (004), (103), and (110) diffraction planes, respectively. Most notably, the two strongest peaks at (002) and (004) represent the perpendicular direction (c-axis) to the hexagonal planes of graphite. These peaks align with reference data for graphite-2h (JCPDS 41-1487).

Transitioning to the XRD spectrum of graphite/LAS (0 kHz), broad diffraction peaks are observed at 2θ = 18°, and sharp peaks at 25.8° - 28.9°. Interestingly, these peaks resemble the pattern seen in reduced graphene oxide (rGO), but with broader peaks. After sonication, the sharp peaks

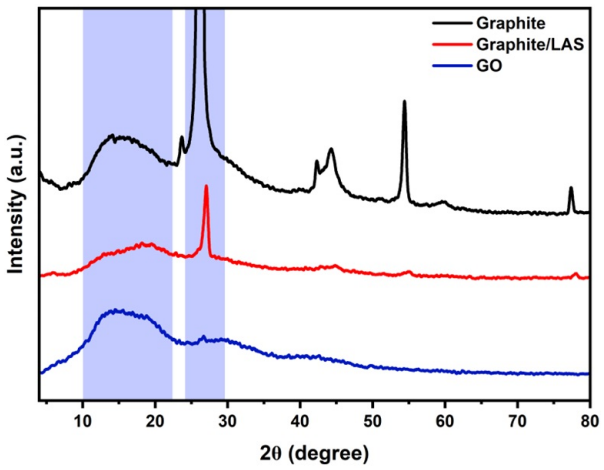

FIG. 5: Diffraction patterns of graphite, graphite/LAS (0 kHz), and GO (21 kHz) samples.

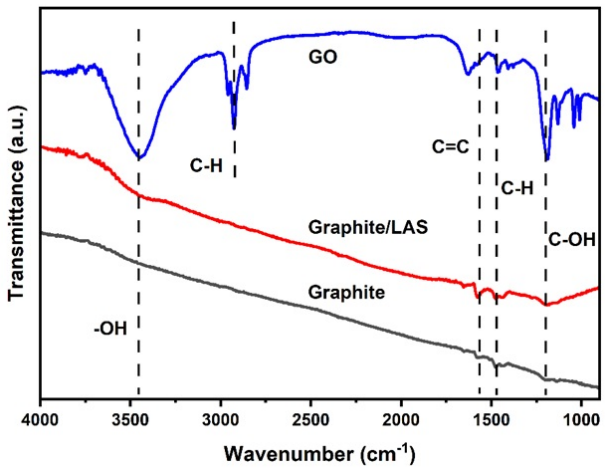

FIG. 6: IR spectra results of graphite, graphite/LAS (0 kHz), and GO (21 kHz) samples.

at 25.8° - 28.9° disappear, leaving broad peaks at 18°, indicating that the synthesized material has an amorphous phase resembling the XRD pattern of GO. The presence of sharp peaks in the graphite XRD pattern and their transformation into broad peaks or disappearance after sonication suggest that the graphite has been exfoliated or the interlayer regions of graphene have been filled with the LAS surfactant.

The broadening of diffraction peaks indicates a decrease in crystallite size. Crystallite size refers to the dimensions of regularly ordered domains within the crystal structure of a material. This crystallite size can be estimated using Gaussian functions applied to the main peaks in the diffraction spectra and calculated using the Debye-Scherrer equation. For graphite, the estimated crystallite size is 15.50 $\pm$ 0.03 nm, which decreases to 0.39 $\pm$ 0.09 nm after the addition of surfactant (0 kHz). The crystallite size of GO increased after the sonication process, but it is still smaller than graphite, measuring 0.8 $\pm$ 0.2 nm. The significant decrease in crystallite size after the addition of surfactant and sonication indicates that the surfactant successfully transforms the crystallinity of graphite into an amorphous material.

The functional group analysis of the graphite, graphite/LAS (0 kHz), and GO (21 kHz) samples conducted using FTIR spectrometer can be seen in Fig. 6. Each functional group exhibits characteristic features at specific wavenumbers, e.g.: single bonds (O-H, N-H, and C-H), triple bonds (CC and CN), double bonds (C=O, C=C, and C=N), and fingerprint region bonds (-CH3, -CH2, C-O, C-N, and C-C) are typically found in the wavenumber ranges of 4000 - 2500 cm^{-1}, 2500 - 2000 cm^{-1}, 2000 - 1500 cm^{-1}, and 1500 - 500 cm^{-1}, respectively. In the FTIR analysis results, it can be observed that the graphite sample exhibits functional groups of C=C, C-H, and C-OH. After the addition of surfactant (0 kHz), the -OH functional group appears indicating the addition of oxygen to the sample. This addition of oxygen occurs because surfactant molecules containing hydroxyl groups adhere to the graphite. After the sonication process, characteristic functional groups of GO such as -OH, C=C, C-H, and C-OH show increased intensities compared to the intensities before sonication [14-16]. This is due to the exfoliation process of graphite into thinner material, resulting in a larger total surface area. The larger surface area allows more surfactant molecules carrying oxygen groups to attach to the surface and interlayer spaces of graphene. The oxygen functional groups on GO make it hydrophilic, hence easier to be dispersed in water.

Fig. 7 depicts the surface morphologies of the graphite, graphite/LAS (0 kHz), and GO (21 kHz) samples at a magnification of 10000X. The graphite sample exhibits a surface morphology of stacked, tangled, and irregularly arranged layers. With the addition of surfactant (0 kHz), the surface morphology appears similar to graphite, but with agglomeration among the layers. A similar morphology is also shown for the GO (21 kHz), where the agglomeration occurring among the layers becomes more apparent. It can be observed that the diameter of graphene layers at the same magnification after sonication becomes smaller. This is due to the cavitation process, which is capable of exfoliating and breaking down graphite into smaller particles.

The elemental compositions of the graphite, graphite/LAS (0 kHz), and GO (21 kHz) samples observed using EDX are shown in Fig. 8. The composition of graphite consists of 95.51% carbon and 6.49% oxygen, with a C/O ratio of 14.7. The addition of surfactant (0 kHz) increases the oxygen composition to 8.75% with the carbon composition of 90.75%, resulting in a C/O ratio of 10.37. After the sonication process (21 kHz), there is an increase in oxygen composition to 11.15%, consistent with the FTIR characterization results due to the increased surface area of GO. The carbon composition after sonication is 68.99%, and the C/O ratio becomes 6.19 with the presence of impurities such as Ti, Na, and Si, possibly caused by the addition of surfactant to the GO. Generally, the C/O ratio for GO falls within the range of 2.12 - 4.9. In this study, the C/O ratio is higher, consistent with the C/O ratio of rGO [21]. The presence of impurities in the sample is also detected at wavelengths of 600-700 nm consistent with the UV-Vis characterization results (see Fig. 2).

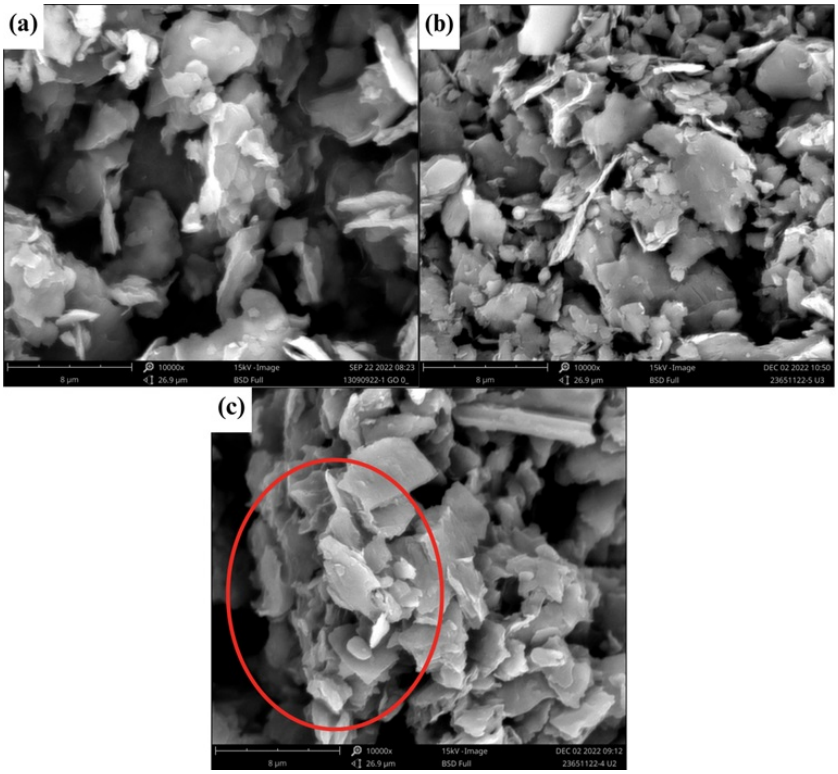

FIG. 7: Surface morphologies of (a) graphite, (b) graphite/LAS (0 kHz), and (c) GO (21 kHz).

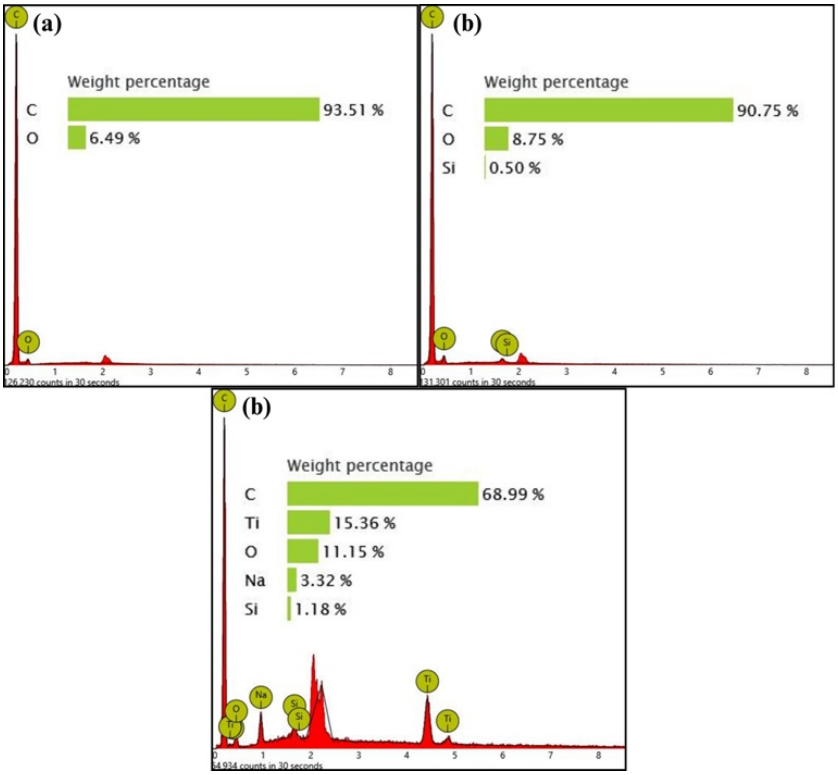

FIG. 8: Elemental compositions of (a) graphite, (b) graphite/LAS, and (c) GO.

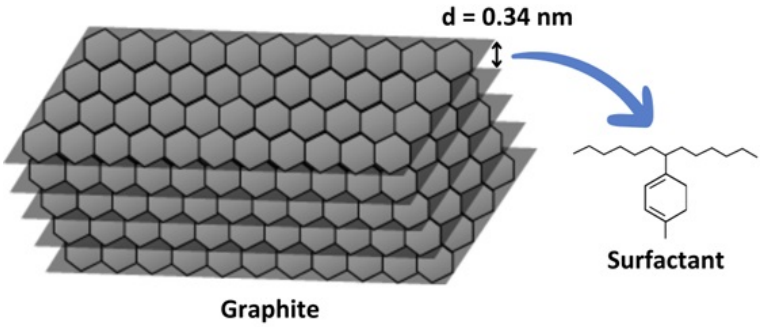

FIG. 9: The role of surfactant in aiding the graphite exfoliation process.

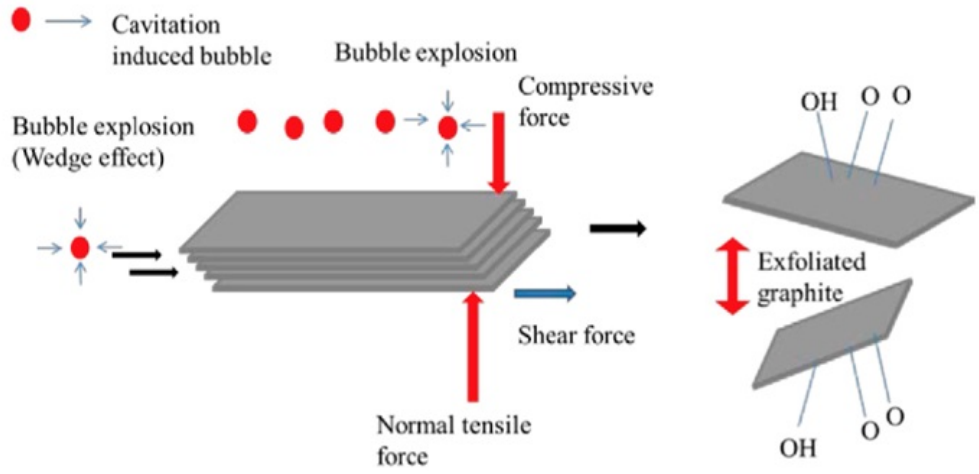

FIG. 10: Illustration of the mechanism of graphite exfoliation utilizing cavitation events [22].

Fig. 9 illustrates the process occurring during the mixing of LAS surfactant into the graphite solution. Surfactants enter the interlayer spaces of graphene material and weaken the van der Waals bonds as shown in Fig. 10. To further understand the exfoliation process during ultrasonic vibration exposure, calculations are performed on the wavelength of the ultrasonic vibration provided. First, the speed of sound in water generated by the ultrasonic cleaner is calculated using the equation,

$$v = \sqrt{\frac{B}{\rho}} \tag{1}$$

where v is the speed of sound, B is the bulk modulus, and ρ is the density of water. Assuming that the bulk modulus of water (B) at normal temperature and pressure is around 2.2×10^9 N/m^2 and the density of water (ρ) at normal temperature and pressure is around 1000 kg/m^3, then from Equation (1), the speed of sound in water is approximately 1484 m/s. Next, we use the equation,

$$\lambda = \frac{v}{f} \tag{2}$$

where λ is the wavelength and f is the frequency of vibration. Now, the frequency of the reactor is given at 21 kHz. By substituting the values of the speed of sound and the frequency of the reaction into Equation (2), the wavelength of the ultrasonic waves in this study is approximately $\lambda \approx 0.0707$ m or $\lambda \approx 70.7$ mm. The significant difference between the wavelength generated by the ultrasonic reactor and the interlayer spacing of graphene, i.e.: 70.7 mm and 0.34 nm, respectively, indicates that the exfoliation process of graphite does not occur solely by utilizing mechanical waves in water. This can be illustrated as graphite particles oscillating in water according to the vibrations generated by the ultrasonic cleaner. However, these particles are only adrift in the fluid without any mechanical force to exfoliate the interlayer graphene sheets as the interlayer spacing is far smaller than the ultrasonic wavelength.

In another study utilizing the ultrasonic method, exfoliation is facilitated by cavitation events. It can be concluded that exposure to ultrasonic vibrations without cavitation events cannot induce graphite exfoliation, as observed in this study's results. Cavitation can be observed through the formation of bubbles in the solution and a significant increase in temperature due to the energy released by cavitation bubbles upon their collapse. Furthermore, cavitation events occur when the intensity and frequency of ultrasonic vibrations reach a certain threshold or can be formulated as the following function:

$$F(I, f) \sim I^{\alpha} \times f^{\beta} \tag{3}$$

where F represents the critical value for exfoliation to occur, I represents the intensity of ultrasonic vibrations. Meanwhile, α and β are certain constant parameters. These two parameters indicate the degree of strength of I and f. Equation (3) indicates that the cavitation process is influenced by the intensity and frequency of the ultrasonic source or ultrasonic vibrations. In this case, we argue that cavitation occurs at ultrasonic frequencies (20 kHz). However, if the intensity of the ultrasonic waves is low, cavitation events may not occur. Thus, there is a certain intensity threshold for cavitation to occur. The results of this study prove that without ultrasonication (0 kHz), where cavitation events do not occur, GO cannot be formed. GO only forms when the ultrasonication process is performed. Therefore, it can be concluded that the addition of LAS surfactant alone is not sufficient to produce GO.

IV. CONCLUSION

In this study, the synthesis of GO using the LPE method based on ultrasonication with LAS surfactant has been successful. Characterizations of the samples through UV-Vis, XRD, FTIR, and SEM-EDX demonstrate the successful synthesis of the GO based on the existence of GO absorption peak characteristics, amorphous phase of the diffraction patterns, oxygen functional groups from the IR spectra, flake morphology from the SEM image, and C/O value of 6.19 from the EDX reslts. The addition of surfactant facilitates the exfoliation of graphite, increasing the amount of oxygen in GO, but surfactant addition alone is not sufficient. Cavitation during sonication with the ultrasonic reactor has proven to be crucial in exfoliating graphite and is a key factor in the successful synthesis of the GO via the LPE method.

Acknowledgments

The authors would like to express their gratitude to the Ministry of Education, Culture, Research, and Technology of Indonesia (KEMDIKBUDRISTEK, Indonesia) for funding this study through the DRTPM scheme 2022.

[1] Y. Zheng, *et al.*, "3D hierarchical graphene oxide-NiFe LDH composite with enhanced adsorption affinity to Congo red, methyl orange and Cr(VI) ions," J. Hazard. Mater., vol. 369, no. February, p. 214-225, 2019, doi: 10.1016/j.jhazmat.2019.02.013.

[2] Y. Hayatgheib, *et al.*, "A comparative study on fabrication of a highly effective corrosion protective system based on graphene oxide-polyaniline nanofibers/epoxy composite," Corros. Sci., vol. 133, no. May 2017, p. 358-373, 2018, doi: 10.1016/j.corsci.2018.01.046.

[3] L.P. Lingamdinne, J.R. Koduru, and R.R. Karri, "A comprehensive review of applications of magnetic graphene oxide based nanocomposites for sustainable water purification," J. Environ. Manage., vol. 231, no. October 2018, p. 622-634, 2019, doi: 10.1016/j.jenvman.2018.10.063.

[4] C. Shuai, *et al.*, "A graphene oxide-Ag co-dispersing nanosystem: Dual synergistic effects on antibacterial activities and mechanical properties of polymer scaffolds," Chem. Eng. J., vol. 347, p. 322-333, 2018, doi: 10.1016/j.cej.2018.04.092.

[5] D. Hu, *et al.*, "Strong graphene-interlayered carbon nanotube films with high thermal conductivity," Carbon N. Y., vol. 118, p. 659-665, 2017, doi: 10.1016/j.carbon.2017.04.005.

[6] F. Li, *et al.*, "Graphene oxide: A promising nanomaterial for energy and environmental applications," Nano Energy, vol. 16, p. 488-515, 2015, doi: 10.1016/j.nanoen.2015.07.014.

[7] N. Cao, and Y. Zhang, "Study of Reduced Graphene Oxide Preparation by Hummers Method and Related Characterization," J. Nanomater., vol. 2015, p. 1-5, 2015, doi: 10.1155/2015/168125.

[8] H. Yu, *et al.*, "High-efficient Synthesis of Graphene Oxide Based on Improved Hummers Method," Sci. Rep., vol. 6, no. November, p. 1-7, 2016, doi: 10.1038/srep36143.

[9] S.M. Notley, "Highly concentrated aqueous suspensions of graphene through ultrasonic exfoliation with continuous surfactant addition," Langmuir, vol. 28, no. 40, p. 14110-14113, 2012, doi: 10.1021/la302750e.

[10] H. Ma, and Z. Shen, "Exfoliation of graphene nanosheets in aqueous media," Ceram. Int., vol. 46, no. 14, p. 21873-21887, 2020, doi: 10.1016/j.ceramint.2020.05.314.

[11] A.V. Tyurnina, *et al.*, "Effects of green solvents and surfactants on the characteristics of few-layer graphene produced by dual-frequency ultrasonic liquid phase exfoliation technique," Carbon N. Y., vol. 206, no. November 2022, p. 7-15, 2023, doi: 10.1016/j.carbon.2023.01.062.

[12] C.X. Hu, *et al.*, "Dispersant-assisted liquid-phase exfoliation of 2D materials beyond graphene," Nanoscale, vol. 13, no. 2, p. 460-484, 2021, doi: 10.1039/d0nr05514j.

[13] H. Gao, *et al.*, "Large-scale graphene production by ultrasound-assisted exfoliation of natural graphite in supercritical CO2/H2O medium," Chem. Eng. J., vol. 308, p. 872-879, 2017, doi: 10.1016/j.cej.2016.09.132.

[14] A.V. Tyurnina, *et al.*, "Ultrasonic exfoliation of graphene in water: A key parameter study," Carbon N. Y., vol. 168, no. 2020, p. 737-747, 2020, doi: 10.1016/j.carbon.2020.06.029.

[15] C.R.C. Rłgo, *et al.*, "Comparative study of van der Waals corrections to the bulk properties of graphite," J. Phys. Condens. Matter, vol. 27, no. 41, p. 415502, 2015, doi: 10.1088/0953-8984/27/41/415502.

[16] B.W. Pratama, and W.S.B. Dwandaru, "Synthesis of reduced graphene oxide based on thermally modified liquid-phase exfoliation," Nano Express, vol. 1, no. 1, p. 1-7, 2020, doi: 10.1088/2632-959X/ab8685.

[17] M.K. Rabchinskii, *et al.*, "Nanoscale perforation of graphene oxide during photoreduction process in the argon atmosphere," J. Phys. Chem. C, vol. 120, no. 49, p. 28261-28269, 2016, doi: 10.1021/acs.jpcc.6b08758.

[18] E.E. Ghadim, *et al.*, "Adsorption properties of tetracycline onto graphene oxide: Equilibrium, kinetic and thermodynamic studies," PLoS One, vol. 8, no. 11, p. 1-9, 2013, doi: 10.1371/journal.pone.0079254.

[19] U.A. Kanta, *et al.*, "Preparations, characterizations, and a comparative study on photovoltaic performance of two different

types of graphene/TiO_2 nanocomposites photoelectrodes," J. Nanomater., vol. 2017, 2017, doi: 10.1155/2017/2758294.

[20] X. Sun, *et al.*, "Enhancing the Performance of PVDF/GO Ultrafiltration Membrane via Improving the Dispersion of GO with Homogeniser," Membranes (Basel), vol. 12, no. 12, p. 1-12, 2022, doi: 10.3390/membranes12121268.

[21] M.P. Arajo, *et al.*, "Tuning the surface chemistry of graphene flakes: new strategies for selective oxidation," RSC Adv., vol. 7, no. 23, p. 14290-14301, 2017, doi: 10.1039/c6ra28868e.

[22] Y. Xu, *et al.*, "Liquid-phase exfoliation of graphene: An overview on exfoliation media, techniques, and challenges," Nanomaterials, vol. 8, no. 11, 2018, doi: 10.3390/nano8110942.